Eur. Phys. J. Spec. Top. (2023) 232:485–497
https://doi.org/10.1140/epjs/s11734-023-00781-0

THE EUROPEAN PHYSICAL JOURNAL SPECIAL TOPICS

Regular Article

Shaping spiking patterns through synaptic parameters as revealed by conventional and wavelet-based bifurcation analysis

Olesia Dogonasheva[1,2,a], Eugene B. Postnikov[3,b], and Anastasia I. Lavrova[5,4,c]

[1] Centre for Cognition and Decision Making, National Research University Higher School of Economics, Krivokolenniy Sidewalk, 3, Moscow 101000, Russia
[2] Group of Neural Theory, École Normale Supérieure PSL University, Rue Lhomond, 24, 75005 Paris, France
[3] Department of Theoretical Physics, Kursk State University, Radishcheva St. 33, Kursk 305000, Russia
[4] Saint-Petersburg State Research Institute of Phthisiopulmonology, Lygovsky Av. 2-4, Saint Petersburg 191036, Russia
[5] Immanuel Kant Baltic Federal University, Nevskogo St. 14, Kaliningrad 236041, Russia

Received 25 October 2022 / Accepted 25 January 2023 / Published online 22 February 2023

Abstract We investigate different dynamical regimes of a small neuronal circuit. This circuit includes two cells that are interconnected by means of dynamical synapses (excitatory and inhibitory). On the individual level, each neuron is modelled by FitzHugh–Nagumo equations. To analyze complex patterns and transitions between them in this small circuit, we apply wavelet analysis. We analyse the influence of synaptic kinetics on the synchronization in this circuit. We also show that the wavelet analysis could be applicable to systems that are difficult to investigate using methods of classical bifurcation analysis.

1 Introduction

Synchronous activity in neuronal networks generates different rhythmic patterns that are responsible for a large variety of physiological processes – from memory to controlling rhythmic movement [1, 2]. Such activity could be presented by the various oscillatory patterns which differ in frequency, amplitude, pattern complexity, simulation thresholds, and localization in the brain (see Reviews, for example, [3–7]). The diversity between regimes is provided by the work of neuronal circuits where the type of coupling (chemical synapse or gap junctions) and its strength [8–11], as well as the structural and physiological properties of neurons, play a crucial role in the establishment of the particular rhythm [1, 12].

Synchronous regimes in neuronal networks could be spontaneous, and transitions between different rhythms are also possible in dependence on the initial conditions or parameters of the system [8, 11, 13]. In numerous experiments and computational simulations, it has been shown that the establishment of different rhythms and switching between them occur due to the control of coupling strengths [11, 14]. Also, it has been shown that the kinetics of synapse as well as the type of synapse, excitatory or inhibitory, influence on the synchronization in neuronal networks, see [13]. Moreover, the kinetics of particular post-synaptic receptors (AMPA, NMDA, GABA) which define a type of synapse, controls the frequency in networks with irregular spiking [15] or can determine the distribution of axons and dendrites [16]. Also, the work of synapse has been considered in detailed models where neurons were described by the equations of Hodgkin–Huxley type [15, 17, 18].

In these models mentioned above, authors consider either the dependence of regimes establishment and transitions between them on the coupling strengths or the influence of synaptic dynamics only on the rhythmogenesis. In view of the aforesaid, some questions arise: can synaptic dynamics be governed by the transitions between different oscillatory states in a network? Does it allow tune-up rhythm transitions more delicately compared with strict changes in coupling strengths? How do the characteristics of synapse kinetics (rise time and time decay of the signal) control the frequency and amplitude of different rhythms?

S.I. : Brain Physiology Meets Complex Systems. Guest editors: Thomas Penzel, Teemu Myllylä, Oxana V. Semyachkina-Glushkovskaya, Alexey Pavlov, Anatoly Karavaev.

[a] e-mail: odogonasheva@hse.ru
[b] e-mail: postnikov@kursksu.ru
[c] e-mail: aurebours@googlemail.com (corresponding author)

The formulation of such problems requires certain methods and tools, due to which it is possible to determine the dynamics of transitions between regimes, e.g. to investigate the continuum of bifurcation patterns transition. Besides classical bifurcation analysis for non-linear systems, one of the most powerful modern tools is the continuous wavelet analysis with complex wavelets [19, 20]. Naturally, it finds a quite wide applications in the field of neuroscience ranged from analysis of experimental data to the revealing non-stationary features in the modelling dynamical system [21]. On the other hand, the majority of such considerations operate with non-intentionally non-stationary non-linear oscillations, while the sequential preparation of neuronal systems for bifurcation study supported by wavelet analysis is only starting to gain research interest. One can note mathematical studies of the neuron-like Bonhoeffer-van der Pol oscillator qualitatively demonstrating the similarity between classic bifurcation diagrams and diagrams of leading wavelet modulus maxima [22], bifurcation-like transitions in the locomotor circadian rhythms induced by gradual changes of the alcohol consumption by rodents [23], wavelet-based analysis of the EEG response on sequential changes of the control parameter for bistable ambiguous images [24]. A preliminary idea to use a non-linear dynamic system with a slowly varying control parameter and give the interpretation of the obtained wavelet transform images in terms of the bifurcational sequence was proposed in [25].

Thus, in view of the above, it would be convenient to consider a system of neurons, taking into account only important dynamical characteristics without a detailed biophysical description. For this purpose, we consider a mini-circuit that consists of the two synaptically coupled neurons (inhibitor and activator) that are described in the frame of the FitzHugh–Nagumo formalism. We intend to give a more solid mathematical basis to the latter approach [25], generalize, and use it for the detailed analysis of the considered system of coupled neuron-like oscillators.

2 Minimal circuit and its model

We consider synaptically coupled basket and pyramidal cells. Figure 1 illustrates the model topology.

The pyramidal and basket cells were described as the FitzHugh–Nagumo model [26] coupled with excitatory and inhibitory chemical synapses:

$$\begin{cases} \dot{v}_i &= v_i - \dfrac{v_i^3}{3} - u_i + I_{\text{ext}}\delta_{i,P} + \sum_j I^{\text{syn}}_{(ji)}, \\ \dot{u}_i &= \epsilon(v_i + a - bu_i), \end{cases} \tag{1}$$

where $i \in \{b, p\}$ is the index of a basket or pyramidal cell, v_i and u_i are the membrane potential and the recovery variable of the i-th neuron, I_{ext} is an external current, parameters a and b mimic ion kinetics, ϵ is a timescale of oscillations, and I^{ji}_{syn} is the synaptic current from cell j to cell i [14, 27]:

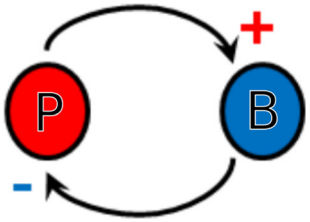

Fig. 1 The model of a coupled basket (B) and pyramidal cells (P). Pyramidal cells are the exciting neurons, basket cells inhibit other neurons [14]. Plus and minus mean positive and negative interconnections

$$\begin{cases} I_{ji} &= G_{ji}s_{ji}(E^{\text{ex}}, \text{in} - v_i), \\ \dot{s}_{ji} &= \frac{A}{2}\Big(1 + \tanh\frac{v_j}{v_{\text{vsl}}}\Big)(1 - s_{ji}) - B_{ji}s_{ji}, \end{cases} \tag{2}$$

where G_{ji} is a coupling strength between elements, $E^{\text{ex,in}}$ is a reversal potential: E^{ex} for excitatory input from pyramidal cell and E^{in} for inhibitory input from basket cell. Synaptic variable s_{ji} depends on a threshold function and defines activation. Parameters A, B_{ji} and v_{vsl} determine synaptic kinetics.

To study what different rhythms arise in dependence on the synaptic variables, we have considered the response of the system to variation of the synaptic parameters B_{pb} and B_{bp}, which determine the kinetic constants of the closed state of excitatory and inhibitory synapses correspondingly. The rest of parameters (parameters of synapse opened state A_{pb} and A_{bp}, potential ν_{vsl}, and constants in the FitzHugh–Nagumo equations) were obtained by fitting experimental data [11, 14, 26] and shown in Table 1.

Therefore, time decay constants B_{pb} and B_{bp} are changed on a grid from 0 to 1, where the starting point is the completely opened synapse state, whereas the last point means an entirely closed state.

Numerical integration of our system (1)–(2) is performed using the fourth-order Runge–Kutta algorithm with a fixed time step of 10 μs.

3 Continuous wavelet transform as a tool for instant bifurcation analysis

Numerical simulations of the system Eqs. (1)–(2) demonstrate a complex dynamical picture, which indicates the existence of non-stationary effects such as hysteresis during forward and backward changes of parameters. Tracing such features related to transitions between different oscillatory regimes, including the changes in the spectral content of non-linear oscillations, is extremely hard, and even sometimes impossible, for conventional methods of bifurcation analysis.

Table 1 Parameters of the model

a	b	ϵ	G_{bp}	G_{pb}	I_{ext}	A	v_{vsl}
0.5	0.8	0.3	0.5	0.5	0.5	1	0.1

Therefore, in this work, we also apply a kind of bifurcation analysis based on the continuous wavelet transform (CWT) with the Morlet wavelet, improving the idea proposed in the work [25].

3.1 From Fourier's to the continuous wavelet transform of limit cycles

The principal idea of the wavelet-bifurcation analysis of transitions between oscillatory states is based on a generalization of the spectral analysis and the respective Andronov's approach [28] to revealing limit cycles. The latter considers a non-linear dynamic system, which can be represented in the complex form as

$$\frac{\mathrm{d}z}{\mathrm{d}t} = i\omega z + \mathscr{Z}(z;\mu), \tag{3}$$

where $z(t) = R\exp(i\omega t)$ is the linear component representing harmonic oscillations with the frequency ω, and $\mathscr{Z}(z;\mu)$ is the non-linear term, with non-linearity governed by the value of the parameter μ ($\mathscr{Z} = 0$ if $\mu = 0$). The existence of a limit cycle with the same period $T_{\mathrm{main}} = 2\pi/\omega$ corresponds to the null-balance of the Fourier component of the non-linear term in Eq. (3), which has the same main frequency ω:

$$\int_0^{2\pi/\omega} \mathscr{Z}(z;\mu)e^{-i\omega t}\mathrm{d}t = 0.$$

Thus, the spectral analysis of dynamical system solutions aimed to reveal its main frequency plays a principal role in the classification of motion with respect to their limit cycles.

At the same time, a spectrum of non-linear oscillations contains a set of peaks: one of them detects the limit cycle period, while the others are higher harmonics, which determine the shape of oscillations.

Since we are interested in the search for limit cycles, it is possible to extract the target oscillatory motion by applying the Gaussian-like window centered at the frequency corresponding to the main period to the full spectrum $\hat{F}[Z(t)]$:

$$\mathscr{F}(\omega) = \hat{F}[Z(t)](\omega)e^{-\frac{\omega_0^2\left(\frac{\omega T_{\mathrm{main}}}{2\pi}-1\right)^2}{2}},$$

where the constant ω_0 is called central frequency; it determines the window's effective width.

Note that this procedure automatically determines the action of the temporal Gaussian sliding window on the original oscillating signal

$$\begin{aligned}\tilde{Z}(t) &= \hat{F}^{-1}[\mathscr{F}(\omega)] \\ &= \int_{-\infty}^{+\infty} Z(t')\frac{e^{-i\omega_0\frac{t'-t}{(\omega_0 T_{\mathrm{main}}/2\pi)}}e^{-\frac{(t'-t)^2}{2(\omega_0 T_{\mathrm{main}}/2\pi)^2}}}{\sqrt{2\pi(\omega_0 T_{\mathrm{main}}/2\pi)^2}}\mathrm{d}t'\end{aligned} \tag{4}$$

due to the convolution theorem.

The procedure represented by Eq. (4) determines local correlations between the harmonic oscillations with the frequency ω and the oscillations cut off from the full curve $Z(t)$ within the relatively short time interval with the characteristic width equal to $\omega_0 T_{\mathrm{main}}/2\pi$. As a result, in the case of non-stationary oscillations, it will produce the signal $\tilde{Z}(t) = [R(t)\exp(i\varphi(t))]\exp(i2\pi t/T_{\mathrm{main}})$ with the same frequency as fast oscillations modulated by the slow-varying complex amplitudes, i.e. an analogue to the van der Pol–Krylov–Bogolyubov method for the slow-fast decomposition (the more detailed consideration of effects of the Gaussian window's width variation, especially in the case of chaotic signals, can be found in the work [29]).

At the same time, more complete information can be obtained by considering the full variety of frequencies (or periods) that are available for determining from a given sample of oscillations. Thus, introducing instead of one fixed period T_{main} the variable $a = (\omega_0/2\pi)T$ called *the scale* and expressed via the possible periods and the central frequency, and the variable b called *the shift*, which determines centering of the variable width sliding window, we get instead of one-dimensional transform (4) the continuous wavelet transform

$$w(a,b) = \int_{-\infty}^{+\infty} Z(t)\psi^*\left(\frac{t-b}{a}\right)\frac{\mathrm{d}t}{a\sqrt{2\pi}} \tag{5}$$

with the standard Morlet wavelet

$$\psi(\xi) = \frac{1}{\sqrt{2\pi}}e^{i\omega_0\xi}e^{-\frac{1}{2}\xi^2}. \tag{6}$$

In Eq. (5), the asterisk denotes the complex conjugation and the normalization factor $1/a\sqrt{2\pi}$ corresponds to the amplitude norm

$$\int_{-\infty}^{+\infty} |\psi(\xi)|\mathrm{d}\xi = 1,$$

which has important advantages from the point of view of extracting periodic components from a signal: (i) for the pure periodic harmonic oscillations $z(t) = \exp(i\omega t)$, its transform has a complex form

$w(a,b) = \exp(i\omega t)\exp\left(-(a\omega-\omega_0)^2/2\right)$, i.e. the frequency may be directly expressed from the maximum of the transform's modulus maximum $\omega = \omega_0/a$ (respectively, the period is equal to $2\pi a/\omega_0$; (ii) the zero-level wavelet transform is exactly proportional to the analysed signal: $w(0,b) = Z(b)\exp\left(-\omega_0^2/2\right)$. These properties assure fast methods for the numerical computing of the CWT and its inversion as well as the interpretation of their results [30, 31].

To operate in the transform (5) with the complex input $Z(t)$ formed as a sum (or an integral in the general continual case) of exponential functions with imaginary exponents and strictly non-negative frequencies, it is convenient to apply the method first proposed by D. Gabor for analysis of non-stationary signals [32] and further effectively transferred to the wavelet theory [33]. It implies the complexification by adding to a real-valued oscillating signal $f(t)$ with extracted its mean constant value its Hilbert transform

$$\mathrm{H}[f(t)](t) = \frac{1}{\pi}\mathrm{v.p.}\int_{\mathbb{R}}\frac{f(t)}{t'-t}\mathrm{d}t'$$

is the imaginary part that results in the analysed function

$$Z(t) = f(t) + i\mathrm{H}[f(t)](t),$$

which has the same set of frequencies but is restricted to the positive values only and additionally implies fast and memory-reducing numerical algorithms for software allowing matrix operations [34].

3.2 Essence of the wavelet-bifurcation analysis

As it is given by Eq. (3), the frequency of limit-cycle oscillations and their amplitudes depend on the value of the control parameter μ. Moreover, when it crosses certain values, bifurcations leading to the change of quantitative properties of the oscillations can occur. However, due to the locality of the continuous wavelet transform, which operates with an effectively limited time range, it is possible to analyse the change of spectral properties of a long sample representing the non-linear oscillations with different values of the parameter μ and to connect these values with the respective main period of the limit-cycle motion (or even with different loops of multi-looped cycles emerging, e.g. due to the period-doubling bifurcations).

For this goal, let us consider the extremely slow (adiabatically) varying time-depended $\mu(t)$. Thus, we will get a non-stationary non-linear oscillations $Z(t;\mu(t))$ within a single run of computing. Quantitatively, this condition can be reached if to define

$$\mu(t) = \mu_0 + kt \tag{7}$$

with

$$\frac{\mathrm{d}\mu(t)}{\mathrm{d}t} = k << \omega = \frac{\omega_0}{\max(a)}, \tag{8}$$

where $\max(a)$ is determined by the upper limit of time scales used during the analysis. Respectively, due to the definition (5)–(6), the non-linearity parameter does not change significantly within the several widths of all applied Gaussian windows included in the Morlet wavelet. Therefore, the output of the CWT will give the complete local spectrum in the vicinity of the instant time, which corresponds to the Gaussian windows centering. The respective instant value of the parameter μ follows from Eq. (8) with this instant time value substituted.

3.3 Smoothing the wavelet modulus maxima in the case of spike sequences

It should be pointed out that dynamical systems mimicking neuronal oscillations reproduce sharp spikes, which are highly non-linear and have a very rich spectral content. Thus, even relatively small central frequencies, which allow for better revealing for the main period of limit-cycle oscillations as the principal wavelet modulus maximum, result in some temporal variation of the letter. This difficulty was indicated in the works [35, 36], where the so-called double-wavelet transform has been proposed. The cited approach applies the CWT to these oscillating wavelet modulus maxima themselves, aimed at the more fine distinction between the slow and fast oscillations and their fine spectral content.

On the other hand, we are interested in the opposite goal, namely, the tracking of the principal period changes, which emerge because of a change of the control parameters in a non-linear system. In this case, we need not enhance and extract oscillations of the wavelet modulus maxima but smooth them. For this reason, we propose an alternative approach via the diffusive smoothing of the non-monotonous wavelet maxima lines defined for each wavelet scale, as the following convolution with the non-oscillating window

$$|\widetilde{w}|^2(a,b) = \int_{-\infty}^{+\infty}|w|^2(a,b)G_\sigma(b-b')\mathrm{d}b', \tag{9}$$

where the Gaussian smoothing window

$$G_\sigma(\xi) = \frac{e^{-\frac{\xi^2}{2\sigma^2}}}{\sqrt{2\pi\sigma^2}}$$

has a width coordinated with the current scale as $\sigma = \pi a/\omega_0$, i.e. the width of this Gaussian is equal to the half-period of oscillations with the wavelet scale a. As a result, the wave bulges and troughs occurring during the oscillation period will be mutually smoothed.

4 Results

As it is known from experiments [11] there are at least three main rhythms that are differed in spike frequency

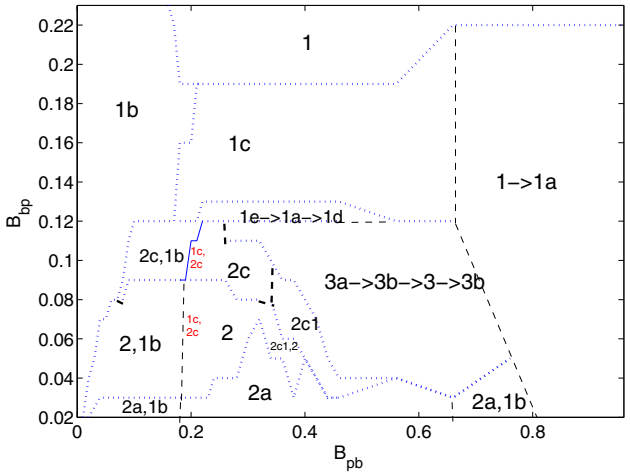

Fig. 2 Map of the dynamical regimes for the system: the numbers correspond to the gamma-rhythm (1), theta rhythm (2), and theta-gamma rhythm (3) while letters denote separate features within each frequency band

and oscillations shape: slow oscillated theta-rhythm (2–11 Hz), gamma rhythm that introduces broad-band (20–100 Hz) and regime where fast rhythm is modulated by slow oscillations, so-called theta/gamma rhythm.

Numerical simulations of the system (1)–(2) reveal all these types in dependence on the parameters B_{pb} and B_{bp} as shown in Fig. 2. In this section, we single out main regimes obtained in model and describe evolution/transformation between them.

4.1 Gamma-rhythm

Gamma rhythm arises at the increasing of two-time decay constants and exists in large intervals of B_{pb} and B_{bp}. A closer look shows that the gamma regime undergoes different transformations in dependence on the parameters' variation: increasing the value B_{bp} at the small values of B_{pb} the gamma regime, where inhibitory cell oscillates subthreshold, whereas excitatory cell gives spikes (regime 1b, see Fig. 2; all further references to regimes mean this figure). This rhythm slowly transforms to classical rhythm gamma (regime 1) at the values of $B_{\mathrm{pb}} > 0.16$ and $B_{\mathrm{bp}} > 0.19$.

The gamma rhythm undergoes period-doubling (regime 1c) within the parameter range $0.18 < B_{\mathrm{pb}} < 0.66$ at the slowly changed parameter B_{bp}. Then this rhythm marked as 1c turns into aperiodic regime (regime 1a) through the sequence of period-doubling bifurcations (regime 1e) that turns into the three-spiking gamma rhythm (1d). These transitions are illustrated by the bifurcation diagrams shown in Fig. 3.

The CWT demonstrates the same picture of transition as seen in its modulus maxima plot shown in Fig. 4. For more direct illustrative purposes, the scale of the wavelet transform corresponding to the main frequencies of the signal's spectral content in this figure as well as in the following CWT-based plots is explicitly expressed in terms of inter-spike intervals (ISI). What is most remarkable is that one can see the chaotic pattern of the transition to the spiking gamma rhythm with the tripling of the period: ISI $\approx 15, 30, 60$ (Fig. 4), where one can distinguish between the preservation of the first spectral band and the fork-like splitting of the spectral band ISI $= 35$ into the bands 30 and 60. The mentioned chaotic-like behaviour is detected within this splitting, which highlights the advantages of the wavelet-bifurcation diagram over the classical one (Fig. 3), where the detailed tracing of the fork's details is not possible.

When the three-spiking gamma rhythm (regime 1d) is changed into the regime 1c ($B_{\mathrm{bp}} \in (0.4386, 0.5515)$) we observe intermittent chaos. The CWT-based picture for it is shown in Fig. 5.

At the further increasing of parameter B_{pb} it changes into chaotic regime (regime 1a) that transforms to the "double-spiking" rhythm (Fig. 6). All these transformations occur within the narrow parameter range $0.11 < B_{\mathrm{bp}} < 0.12$.

At the $B_{\mathrm{pb}} > 0.8$, the classical gamma rhythm appears (the zone $1 \to 1a$, the left-hand side of the diagram shown in fig:map) that undergoes the sequence of transformations. This transformation also goes through chaos (Fig. 7).

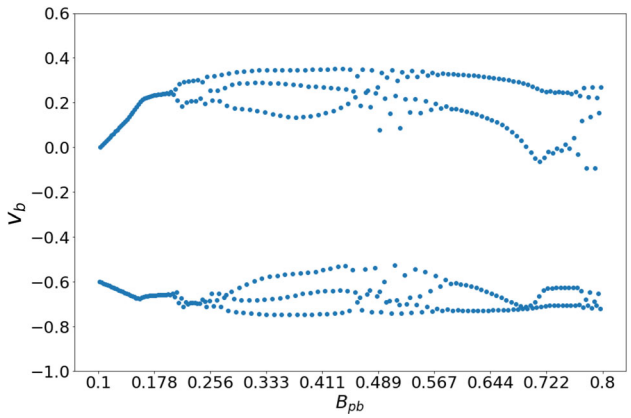

Fig. 3 Bifurcation diagram for $B_{\mathrm{pb}} \in (0.1, 0.8)$ and fixed $B_{\mathrm{bp}} = 0.12$. Here dots correspond to the extremum values of the function v_b

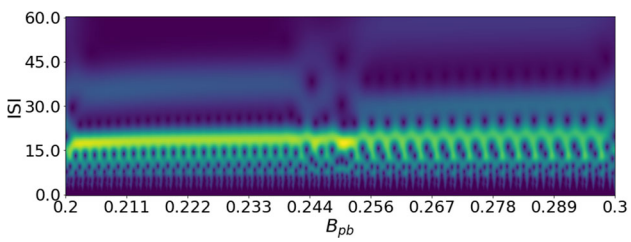

Fig. 4 Wavelet transform's modulus for the parameters $B_{\mathrm{bp}} = 0.12$, $B_{\mathrm{pb}} \in (0.2, 0.3)$. Bright yellow colouring marks the wavelet maxima lines

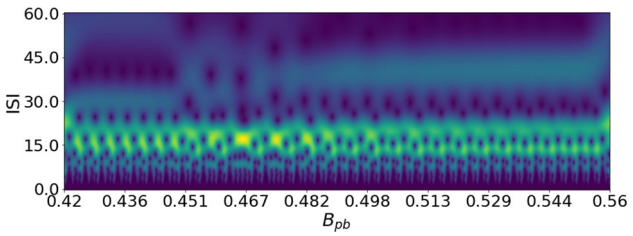

Fig. 5 Wavelet transform's modulus for the parameters $B_{\mathrm{pb}} = 0.12$, $B_{\mathrm{pb}} \in (0.4, 0.5)$. Bright yellow colouring marks the wavelet maxima lines

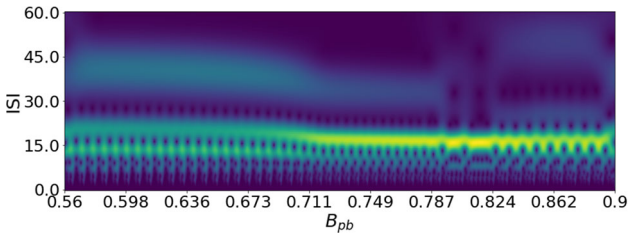

Fig. 6 Wavelet transform's modulus for the parameters $B_{\mathrm{pb}} = 0.12$, $B_{\mathrm{pb}} \in (0.5, 0.9)$. Bright yellow colouring marks the wavelet maxima lines

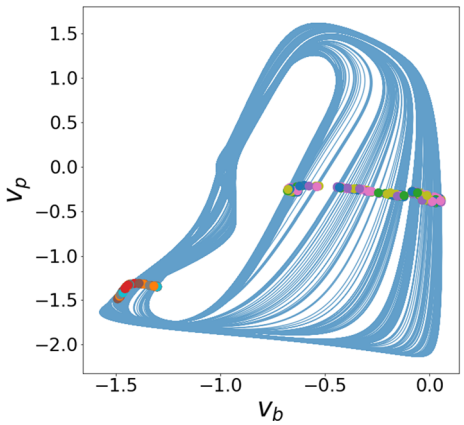

Fig. 7 Poincare section and phase portrait of chaotic behaviour for $B_{\mathrm{bp}} = 0.12$, $B_{\mathrm{pb}} = 0.79$

4.2 Theta rhythm

The aperiodic theta rhythm (regime 2a) is replaced by the conventional theta rhythm (regime 2) at the values of $0.03 < B_{\mathrm{bp}} < 0.09$ within the interval of B_{pb} ranged from 0.02 to 0.4; the characteristic time duration of one oscillation gradually decreases from ≈ 340 to 51. At the $B_{\mathrm{bp}} > 0.09$ the period abruptly falls to values 36–37, and the regime close to theta rhythm arises (regime 2c). The transition from regime 2 to regime 2c includes hysteresis, which is highlighted in the wavelet-bifurcation diagram shown in Fig. 8. This picture of the hysteresis was calculated referring to the wavelet modulus maxima determined from the CWT of signals with the bifurcation parameter slowly varying with time starting from values, which correspond to the opposite values in the considered range.

We observe the limit cycle with the loop ($T = 56$) for $B_{\mathrm{bp}} = 0.06-0.0849$. When B_{bp} comes to the vicinity of the value 0.085, the loop disappears through the chaotic pattern and we can observe the limit cycle with the period $T = 39$. Transition when $B_{\mathrm{pb}} = 0.19$ and $B_{\mathrm{bp}} = 0.079 - 0.086$ are shown in Fig. 9.

For this range of the parameter, we can observe a clearly chaotic behaviour. To confirm this, the Poincare section for $B_{\mathrm{pb}} = 0.19$ and $B_{\mathrm{bp}} = 0.079-0.086$ is shown in Fig. 10.

The regime 2c at the $B_{\mathrm{pb}} > 0.33$ is replaced (through a sequence of aperiodic regimes) by the theta regime where the inhibitory cell oscillates in the subthreshold regime (the regime 2c1). Let us consider this replacement in more detail. The regime 2c is characterised by the period $T = 51$. These oscillations continue up to $B_{\mathrm{pb}} = 0.27$. For the parameter range $B_{\mathrm{pb}} \in (0.27, 0.295)$, we observe period-doubling bifurcations leading to a chaotic pattern (Fig. 11).

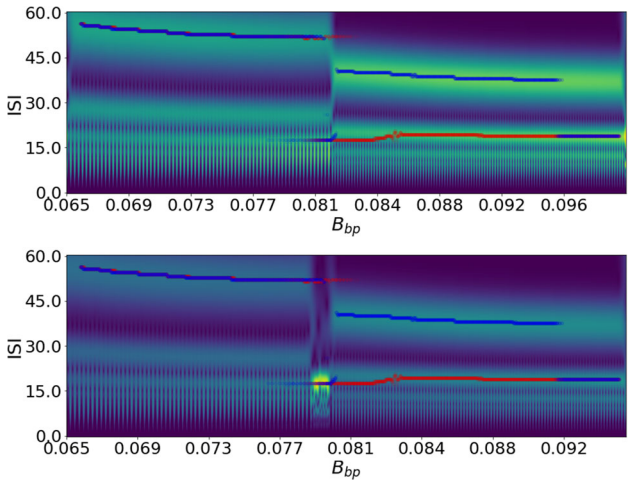

Fig. 8 Top panel: the hysteresis indicated in the wavelet modulus maxima lines in direct pass (red line). Bottom panel: the hysteresis indicated in the wavelet modulus maxima lines (blue line). The fixed parameter: $B_{\mathrm{pb}} = 0.19$. The range of the parameter's variation: $B_{\mathrm{bp}} = 0.06..0.1$

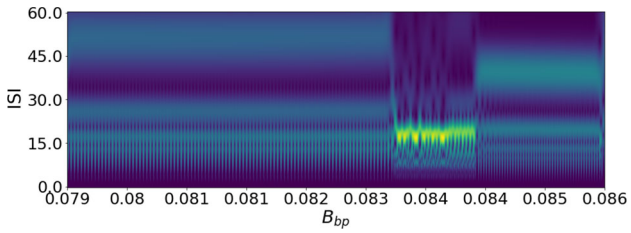

Fig. 9 Transition with a chaotic pattern. The fixed parameter: $B_{\mathrm{pb}} = 0.19$. The variable parameter: $B_{\mathrm{bp}} = 0.079..0.086$

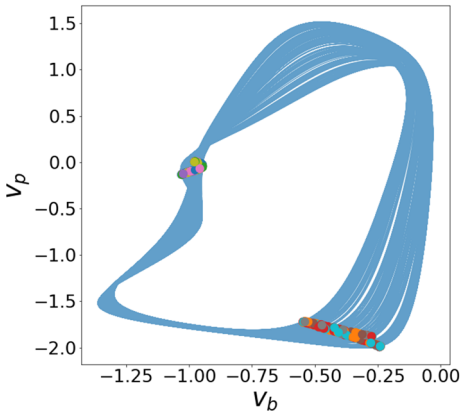

Fig. 10 Poincare section and example of the respective chaotic attractor for $B_{\text{pb}} = 0.19$ and $B_{\text{bp}} = 0.084$

To be sure that we have already found chaos, we calculated the maximal Lyapunov exponent for the parameter $B_{\text{pb}} = 0.27$: $\lambda = 0.004$ (std $= 0.0019$). This transition leads to the loop's disappearing and emerging oscillations with the period $T = 32.4$.

After chaotic oscillations, the system comes to regime 2c. The region of this rhythm is located in a narrow range of parameters, namely $0.34 < B_{\text{pb}} < 0.42$ and $0.03 < B_{\text{bp}} < 0.09$.

4.3 Theta-gamma rhythm

Finally, let us consider the transformations of theta rhythms when parameter B_{pb}, which describes the exciting synapse, changes (the sequence leading to the chain of regimes 3a → 3b → 3 → 3b. If we continue increasing B_{pb} greater than 0.33, a loop on the limit cycle appears. Figure 12 shows the gradual loop appearance.

After loop rolling, we observe a series of period-doubling bifurcations (Fig. 13), which ends with a chaotic attractor at $B_{\text{pb}} = 0.3781$. The maximal Lyapunov exponent is equal to $\lambda = 0.018$ (std $= 0.003$).

The chaotic nature of the oscillations changes to another kind of complex oscillations for $B_{\text{pb}} = 0.380$ ($T = 121$, $ISI = 30$) with the subsequent transformation into the theta-gamma rhythm for $B_{\text{pb}} = 0.448$.

For $B_{\text{pb}} = 0.4490$, we observe period-doubling bifurcations that ends with chaos for $B_{\text{pb}} = 0.4550$: $\lambda = 0.0224$, std $= 0.0058$. The chaotic pattern is replaced by the stable theta-gamma rhythm for $B_{\text{bp}} \in (0.456, 0.461)$.

The range $B_{\text{pb}} \in (0.4615, 0.4897)$ consists of states with a lot of chaotic transitions between different regimes. Figure 14 demonstrates diversity of regimes for this range.

For $B_{\text{pb}} \in (0.491, 0.71)$, we observe the stable theta-gamma rhythm (Fig. 15).

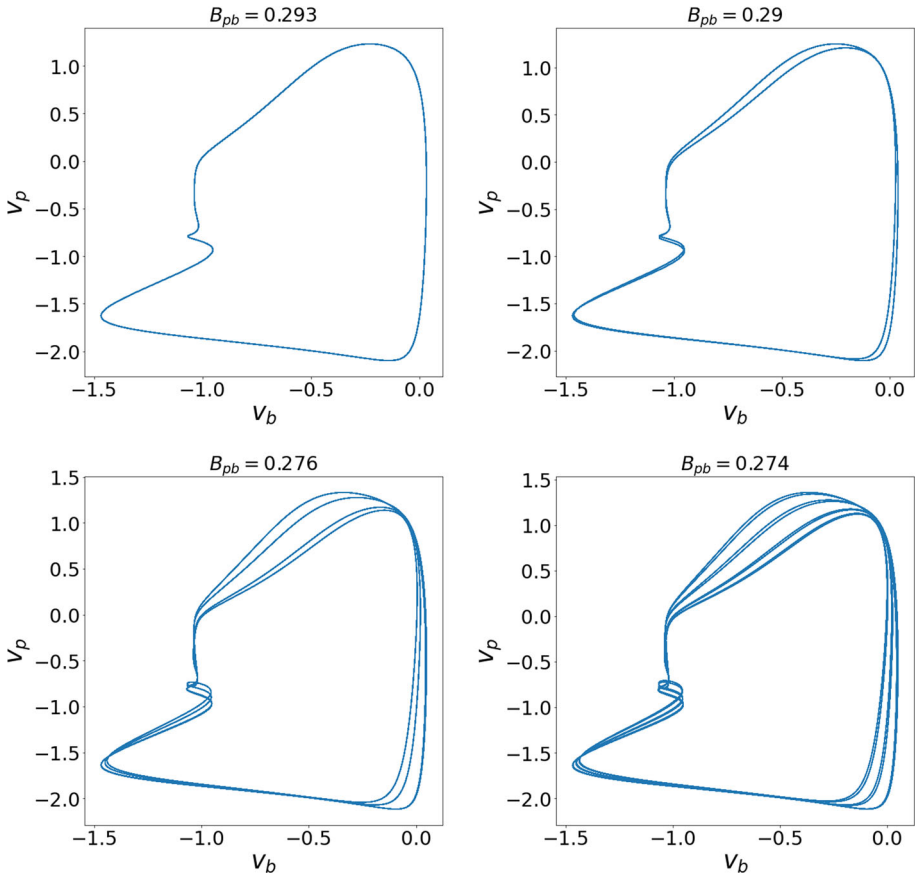

Fig. 11 Period doubling bifurcation. Synaptic parameter $B_{\text{bp}} = 0.08$ is fixed and $B_{\text{pb}} = 0.293$, $B_{\text{pb}} = 0.290$, $B_{\text{pb}} = 0.276$, $B_{\text{pb}} = 0.274$

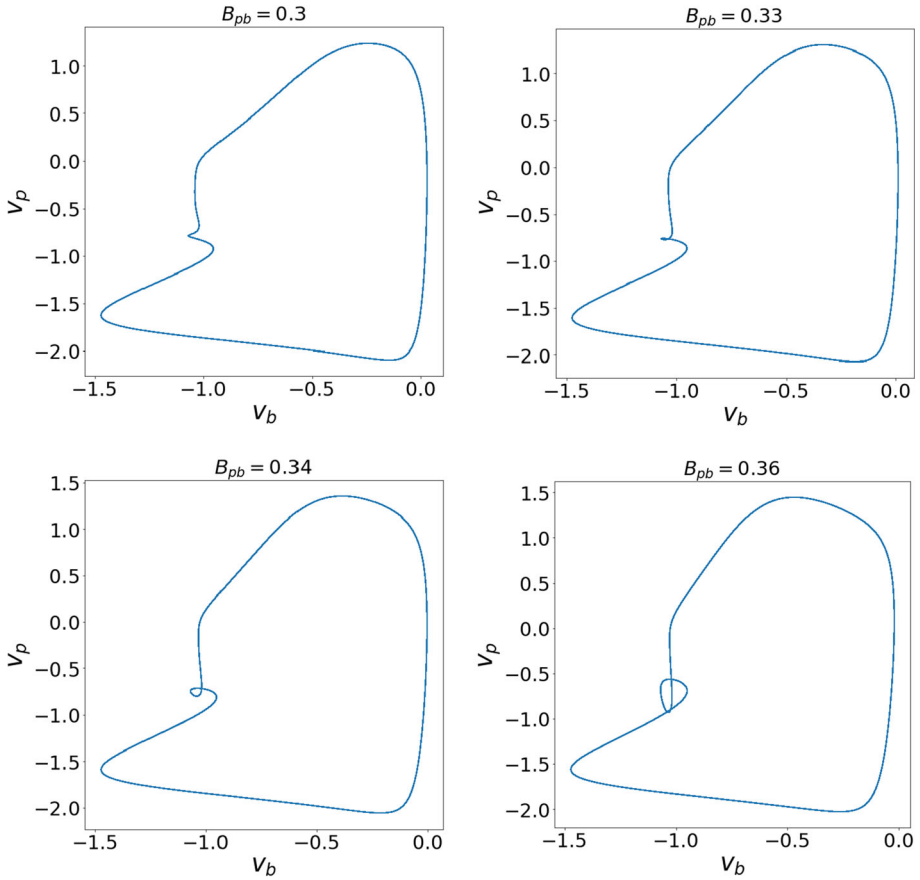

Fig. 12 Loop rolling. Synaptic parameter $B_{\mathrm{bp}} = 0.08$ is fixed and $B_{\mathrm{pb}} = 0.30$, $B_{\mathrm{pb}} = 0.33$, $B_{\mathrm{pb}} = 0.34$, $B_{\mathrm{pb}} = 0.36$

For $B_{\mathrm{pb}} \in (0.7, 0.82)$ we observe complex behaviour with chaotic patterns for (Fig. 16).

4.4 Multistability

Note that, as it is demonstrated above, the solution of the system (1)–(2) exhibits hysteresis and specific transitions between particular spectral bands contained in the spikes of complex shape depending on the paths of change of bifurcation parameters as revealed by the wavelet-bifurcation diagrams. Thus, the system exhibits multistability.

To get the respective classification of the rhythms, we imply the calculation of the minimal and maximal ISI. If the maximal and minimal ISI differed by more than two times, we supposed it was a theta-gamma regime. In this case, the maximal ISI corresponded to the interburst interval (IBI). On the contrary, pure gamma and theta rhythms can be distinguished by the ISI value only. Using this approach, we calculated the map of the rhythms with fixed initial conditions. Since the system is multistable, we had to find all the possible states for each parametric set. To simplify this task, we found the boundaries on the map with fixed initial conditions for each rhythm. Then we expanded these boundaries as follows: we calculated dynamics where the last step was used as the initial conditions. The resulting map is presented in Fig. 17, where one can see both monostable regimes (a single-type patterning) as well as the regions of multistability, where different kinds of patterning overlap.

5 Discussion

Although the key role of gamma and theta rhythms and their coupling is a well-established mechanism of the brain's activity related to a wide variety of processes related to memory, spatial navigation, etc. [37–39], the understanding of this stitching's regulation and the development of the respective mathematical models are still far from the completeness. To achieve the required dynamical picture, the most recent models operate with a large ensemble of neuronal oscillators and consider theta-gamma switches as a consequence of complex network dynamics [40–42]. At the same time, it has been demonstrated that switching between frequency bands, including multistable dynamics, can be observed in more simple models, which include a few neuronal cells. In particular, in the work [43], a variant of regime switching was achieved with two neurons and two astrocytes, which govern synaptic transmission.

In our work, we deal with the minimal possible model system, which includes only two synaptically coupled neurons. It turns out that the specificity of synaptic

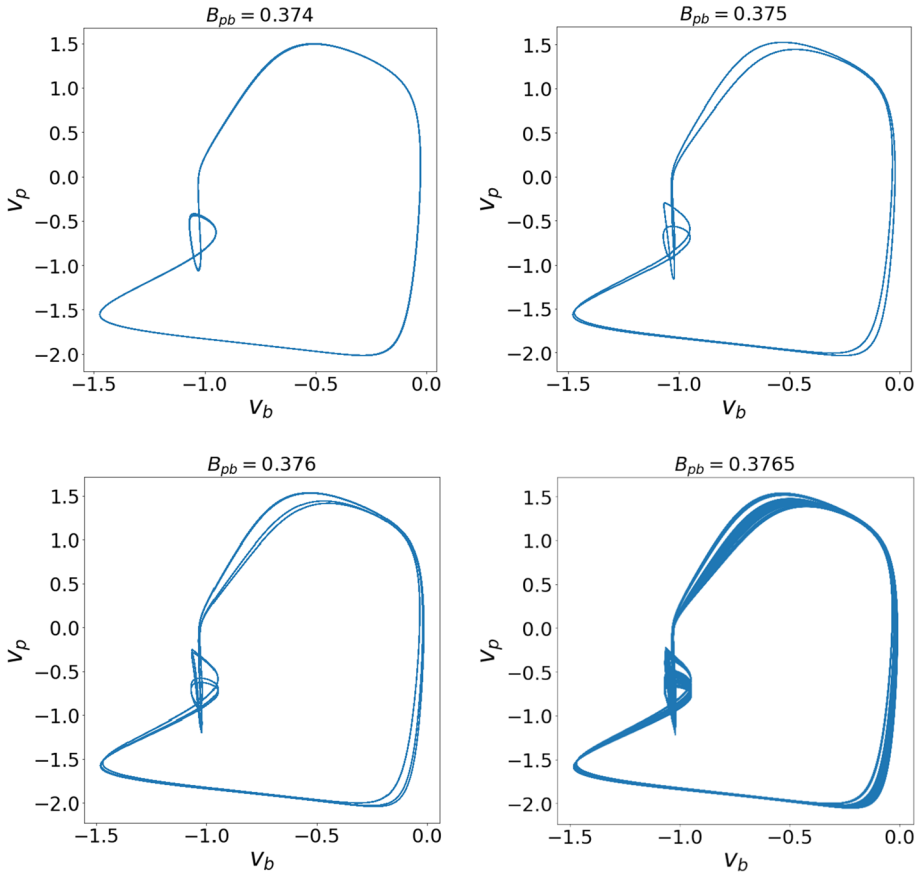

Fig. 13 Period doubling bifurcation. Synaptic parameter $B_{\mathrm{bp}} = 0.08$ is fixed and $B_{\mathrm{pb}} = 0.3740$, $B_{\mathrm{pb}} = 0.3750$, $B_{\mathrm{pb}} = 0.3760$, $B_{\mathrm{pb}} = 0.3770$

coupling is quite enough to produce the full range of a variety of dynamical regimes that are qualitatively comparable with those that were observed in neurobiological experiments. Thus, this result shifts attention from large and complex (and, as a consequence, not very interpretable) networks to more plausible mechanisms of inter-neuronal interactions.

Alongside the building of mathematical models of these inter-neuronal interactions, there is a special question about the analysis of the dynamics of such a highly nonlinear coupled system, which is rather complex. New methods that use the wavelet transform can provide more opportunities for this goal.

It should be pointed out that although the wavelet transform has recently become part of the standard protocols for rhythms and chaos investigations in biology [44], its widespread application is mostly limited by the detection of rhythms in time series. Applications from the point of view of the bifurcation analysis are scarce [22, 45, 46] and mainly address again wavelets as a tool for characterising complex dynamics of time series generated by the system with some fixed parameters. This means that building the bifurcation diagram based on the characteristics revealed by the analysis of time series generated by a nonlinear system at some set of parameters is still computationally expensive because it requires generating long time series for each point in the parametric space. On the contrary, the proposed wavelet-bifurcation approach is free of such a drawback since the simultaneous change of the parameter and the time of observations allows getting a picture of transitions during one run of time series calculations.

In addition, the proposed method provides an opportunity to address the question of the dynamics of transitions as a function of the rate of parameter change. Recently, this problem has attracted active attention within the context of the transition delay effect and early warnings of catastrophic systemic restructuring in nonlinear systems [47–50]. Such effects can be extremely hard (if even possible) to detect with the usual methods of bifurcation analysis due to operating with a set of fixed values for bifurcation parameters. But the wavelet-bifurcation method, which we proposed, operates with the required conditions by construction. In particular, we demonstrated some practical examples of the considered multistable system.

6 Conclusions

The main messages of this work can be summarised as twofold.

First of all, we demonstrated that even a system of only two coupled identical neurons can exhibit a rich variety of dynamic regimes that cover all three principal spectral bands of neuronal oscillations. The main premise of such a possibility is a non-symmetrical

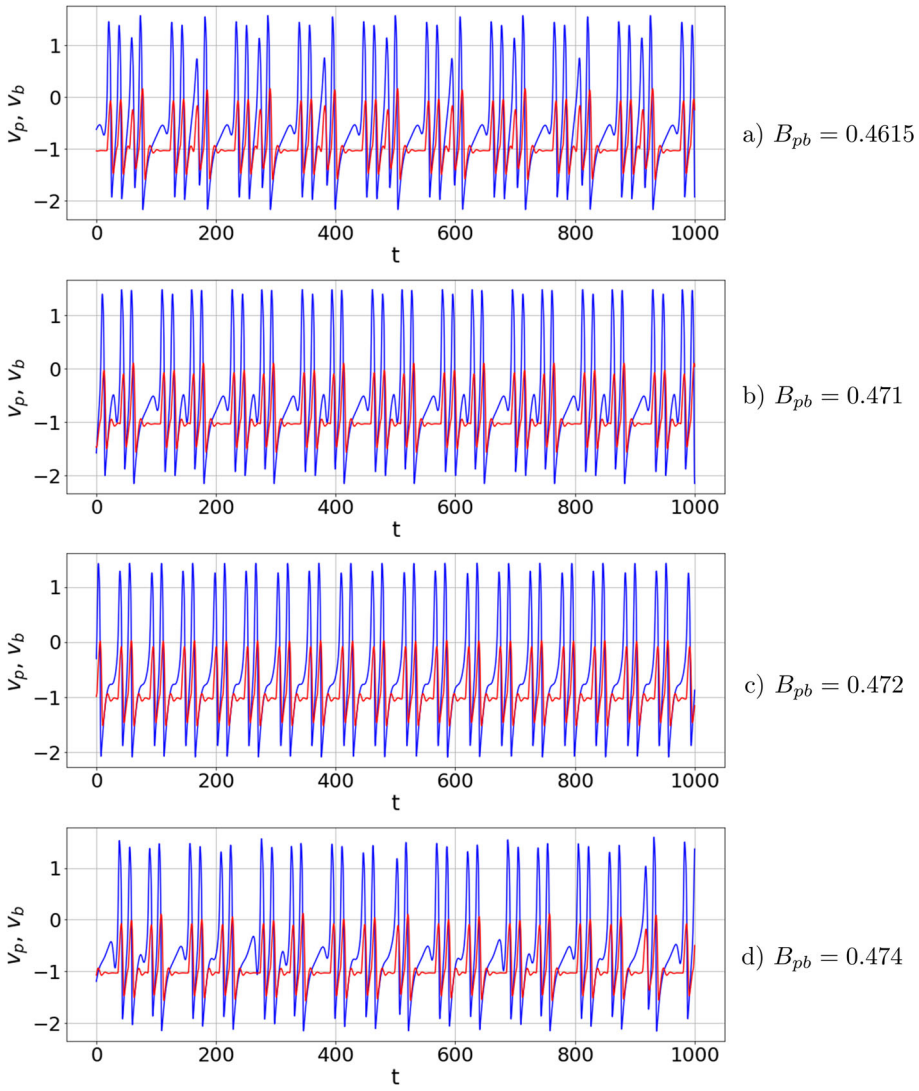

Fig. 14 Diversity of oscillatory regimes for the synaptic parameter's range $B_{\mathrm{pb}} \in (0.4615, 0.4897)$. The synaptic parameter $B_{\mathrm{bp}} = 0.08$ is fixed. Red and blue colors mark ν_b and ν_p

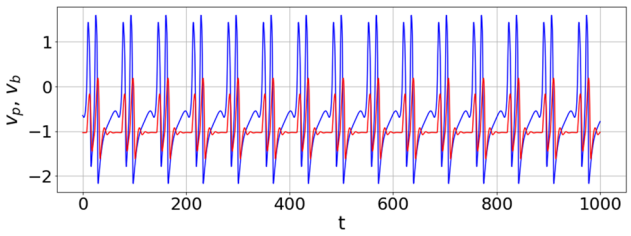

Fig. 15 Theta-gamma oscillations for $B_{\mathrm{pb}} \in (0.491, 0.71)$ and fixed $B_{\mathrm{bp}} = 0.08$. Red and blue colors mark ν_b and ν_p correspondingly

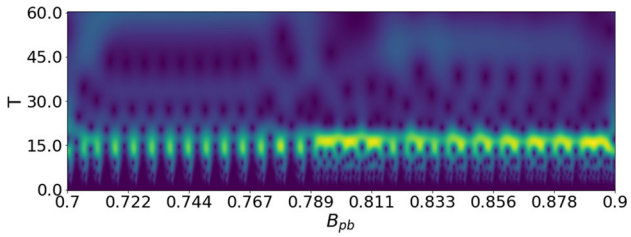

Fig. 16 Wavelet transform's modulus for the parameters for $B_{\mathrm{pb}} \in (0.7, 0.9)$ and fixed $B_{\mathrm{bp}} = 0.08$. Bright yellow colouring marks the wavelet maxima lines

coupling, with the strength determined by the kinetic parameters of the connection. Thus, we can conclude that this provides some open questions for future neurobiological studies aimed at clarifying whether the large systems of coupled neurons are already underlying neuronal activity as indicated by the change of gamma and theta regimes or whether such neuronal tasks can be carried out by extremely small groups of neurons by adjusting the coupling between them.

The second message relates to more procedural aspects of the work. It is known that bifurcation analysis of periodic orbits is a very complicated procedure for the vast majority of conventionally used algorithms and implementing them in programs (such as LOCBIF,

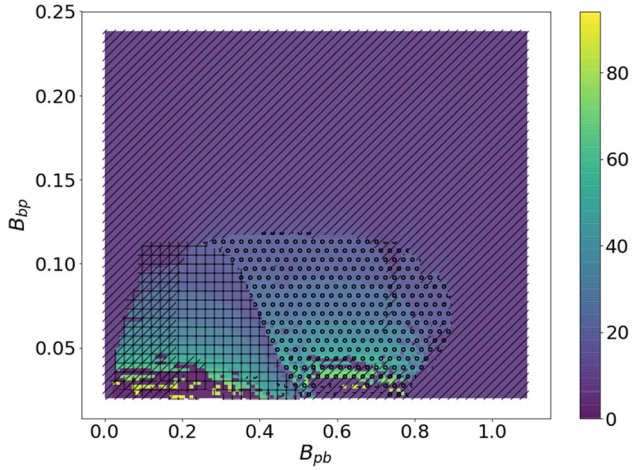

Fig. 17 Multistability map. The diagonal hatch corresponds to the gamma rhythm, the squared hatch corresponds to the theta rhythm, the circled texture corresponds to the theta-gamma rhythm. Colormap presents ISI for the theta and gamma rhythm and IBI for the theta-gamma rhythm

MatCont, etc.). In cases when one is interested in multistable transitions between particular spectral components of multi-loop (in the phase space representation) oscillations, such conventional analysis can be even impossible. On the contrary, the wavelet-bifurcation approach, which operates with the continuous revealing changes in the instant period of spikes under conditions of a slowly varying bifurcation parameter, solves this problem easily because it falls directly into the CWT's focusing point. In addition, the cross-section over the wavelet scales (equivalent to the interspike intervals after proper scaling) at each time/instant parameter value indicates principal components of the spike's shape, whose bifurcations can be studied separately from the spike trains considered as a whole. Thus, the wavelet-bifurcation analysis, which inherits Andronov's approach to the limit cycle decomposition but supplies it with the property of time/parameter locality, calls for new insight in the practical study of the evolutionary dynamics of strongly non-linear systems.

Acknowledgements AIL was supported by the Project of the state assign of the Ministry of Education and Science of the Russian Federation No. 75-02-2022-872

Data availability statement Not applicable.

Declarations

Conflict of interest We declare no conflict of interest.

References

1. G. Buzsáki, A. Draguhn, Neuronal oscillations in cortical networks. Science **304**, 1926–1929 (2004). https://doi.org/10.1126/science.1099745
2. S. Grillner, H. Markram, E. De Schutter, G. Silberberg, F.E.N. LeBeau, Microcircuits in action-from CPGs to neocortex. Trends Neurosci. **28**, 525–533 (2005). https://doi.org/10.1016/j.tins.2005.08.003
3. P. Sauseng, W. Klimesch, What does phase information of oscillatory brain activity tell us about cognitive processes? Neurosci. Biobehav. Rev. **32**, 1001–1013 (2008). https://doi.org/10.1016/j.neubiorev.2008.03.014
4. J.B. Caplan, J.R. Madsen, S. Raghavachari, M.J. Kahana, Distinct patterns of brain oscillations underlie two basic parameters of human maze learning. J. Neurophysiol. **86**, 368–380 (2001). https://doi.org/10.1152/jn.2001.86.1.368
5. M. Garcia-Munoz, L. Carrillo-Reid, G.W. Arbuthnott, Functional anatomy: dynamic states in basal ganglia circuits. Front. Neuroanat. **4**, 144 (2010). https://doi.org/10.3389/fnana.2010.0014
6. A.K. Engel, C. Gerloff, C.C. Hilgetag, G. Nolte, Intrinsic coupling modes: multiscale interactions in ongoing brain activity. Neuron **80**, 867–886 (2013). https://doi.org/10.1016/j.neuron.2013.09.038
7. M.J. Kahana, The cognitive correlates of human brain oscillations. J. Neurosci. **26**, 1669–1672 (2006). https://doi.org/10.1523/JNEUROSCI.3737-05c.2006
8. G. Buzsáki, Neural syntax: cell assemblies, synapsembles, and readers. Neuron **68**, 362–385 (2010). https://doi.org/10.1016/j.neuron.2010.09.023
9. A. Szücs, F. Berton, T. Nowotny, P. Sanna, W. Francesconi, Consistency and diversity of spike dynamics in the neurons of bed nucleus of stria terminalis of the rat: a dynamic clamp study. PLoS ONE **5**, 11920 (2010). https://doi.org/10.1371/journal.pone.0011920
10. C.T. Dickson, Ups and downs in the hippocampus: the influence of oscillatory sleep states on "neuroplasticity" at different time scales. Behav. Brain Res. **214**, 35–41 (2010). https://doi.org/10.1016/j.bbr.2010.04.002
11. T. Gloveli, T. Dugladze, H.G. Rotstein, R.D. Traub, H. Monyer, U. Heinemann, M.A. Whittington, N.J. Kopell, Orthogonal arrangement of rhythm-generating microcircuits in the hippocampus. Proc. Natl. Acad. Sci. USA **102**, 13295–13300 (2005). https://doi.org/10.1073/pnas.0506259102
12. O. Sporns, G. Tononi, G.M. Edelman, Connectivity and complexity: the relationship between neuroanatomy and brain dynamics. Neural Netw. **13**, 909–922 (2000). https://doi.org/10.1016/S0893-6080(00)00053-8
13. S.T. Alford, M.H. Alpert, A synaptic mechanism for network synchrony. Front. Cell. Neurosci. **8**, 290 (2014). https://doi.org/10.3389/fncel.2014.00290
14. A.I. Lavrova, M.A. Zaks, L. Schimansky-Geier, Modeling rhythmic patterns in the hippocampus. Phys. Rev. E **85**, 041922 (2012). https://doi.org/10.1103/PhysRevE.85.041922
15. N. Brunel, X.-J. Wang, What determines the frequency of fast network oscillations with irregular neural discharges? I. Synaptic dynamics and excitation-inhibition balance. J. Neurophysiol. **90**, 415–430 (2003). https://doi.org/10.1152/jn.01095.2002

16. R. Cossart, Z. Petanjek, D. Dumitriu, J.C. Hirsch, Y. Ben-Ari, M. Esclapez, C. Bernard, Interneurons targeting similar layers receive synaptic inputs with similar kinetics. Hippocampus **16**, 408–420 (2006). https://doi.org/10.1002/hipo.20169
17. L. Wang, S.T. Kitai, Z. Xiang, Activity-dependent bidirectional modification of inhibitory synaptic transmission in rat subthalamic neurons. J. Neurosci. **26**, 7321–7327 (2006). https://doi.org/10.1523/JNEUROSCI.4656-05.2006
18. Z. Wang, H. Fan, F. Han, A new regime for highly robust gamma oscillation with co-exist of accurate and weak synchronization in excitatory-inhibitory networks. Cogn. Neurodyn. **8**, 335–344 (2014). https://doi.org/10.1007/s11571-014-9290-4
19. S. Mallat, *A Wavelet Tour of Signal Processing. The Sparse Way* (Academic Press, Burlington, 2009). https://doi.org/10.1016/B978-0-12-374370-1.X0001-8
20. P.S. Addison, *The Illustrated Wavelet Transform Handbook: Introductory Theory and Applications in Science, Engineering, Medicine and Finance* (CRC Press, Boca Raton, 2017). https://doi.org/10.1201/9781315372556
21. A.E. Hramov, A.A. Koronovskii, V.A. Makarov, V.A. Maximenko, A.N. Pavlov, E. Sitnikova, *Wavelets in Neuroscience* (Springer, Berlin–Heidelberg, 2021). https://doi.org/10.1007/978-3-030-75992-6
22. R. Benítez, V.J. Bolós, M.E. Ramírez, A wavelet-based tool for studying non-periodicity. Comput. Math. Appl. **60**, 634–641 (2010). https://doi.org/10.1016/j.camwa.2010.05.010
23. J.C. Foo, H.R. Noori, I. Yamaguchi, V. Vengeliene, A. Cosa-Linan, T. Nakamura, K. Morita, R. Spanagel, Y. Yamamoto, Dynamical state transitions into addictive behaviour and their early-warning signals. Proc. Roy. Soc. B Biol. Sci. **284**, 20170882 (2017). https://doi.org/10.1098/rspb.2017.0882
24. V.A. Maksimenko, A.E. Runnova, M.O. Zhuravlev, V.V. Makarov, V. Nedayvozov, V.V. Grubov, S.V. Pchelintceva, A.E. Hramov, A.N. Pisarchik, Visual perception affected by motivation and alertness controlled by a noninvasive brain–computer interface. PLoS ONE **12**, 0188700 (2017). https://doi.org/10.1371/journal.pone.0188700
25. E.B. Postnikov, A.I. Lavrova, R.V. Kiseliov, T.Y. Plyusnina, Wavelet bifurcation analysis of dynamical systems: a case study in oscillations of Chara corallina transmembrane potential. Int. J. Bifurc. Chaos **22**, 1250293 (2012). https://doi.org/10.1142/S0218127412502938
26. R. FitzHugh, Impulses and physiological states in theoretical models of nerve membrane. Biophys. J . **1**, 445–466 (1961). https://doi.org/10.1016/S0006-3495(61)86902-6
27. V. Cutsuridis, B. Graham, S. Cobb, I. Vida (eds.) Hippocampal Microcircuits: A Computational Modeler's Resource Book (Springer, New York, 2010). https://doi.org/10.1007/978-1-4419-0996-1
28. A.A. Andronov, Les cycles limites de Poicaré et la théorie des oscillations auto-entrenues. CR Acad. Sci. Paris **189**, 559–561 (1929)
29. E.B. Postnikov, Wavelet phase synchronization and chaoticity. Phys. Rev. E **80**, 057201 (2009). https://doi.org/10.1103/PhysRevE.80.057201
30. E.A. Lebedeva, E.B. Postnikov, On alternative wavelet reconstruction formula: a case study of approximate wavelets. Roy. Soc. Open Sci. **1**, 140124 (2014). https://doi.org/10.1098/rsos.140124
31. E.B. Postnikov, E.A. Lebedeva, A.I. Lavrova, Computational implementation of the inverse continuous wavelet transform without a requirement of the admissibility condition. Appl. Math. Comput. **282**, 128–136 (2016). https://doi.org/10.1016/j.amc.2016.02.013
32. D. Gabor, Theory of communication. Part 1: the analysis of information. J. Inst. Electr. Eng.-Part III Radio Commun. Eng. **93**, 429–441 (1946). https://doi.org/10.1049/ji-3-2.1946.0074
33. M. Duval-Destin, M.A. Muschietti, B. Torrésani, Continuous wavelet decompositions, multiresolution, and contrast analysis. SIAM J. Math. Anal. **24**, 739–755 (1993). https://doi.org/10.1137/0524045
34. E.B. Postnikov, M.O. Tsoy, M.A. Kurochkin, D.E. Postnov, A fast method for the detection of vascular structure in images, based on the continuous wavelet transform with the Morlet wavelet having a low central frequency. Proc. SPIE **10337**, 103370 (2017). https://doi.org/10.1117/12.2268427
35. O.V. Sosnovtseva, A.N. Pavlov, E. Mosekilde, N.-H. Holstein-Rathlou, D.J. Marsh, Double-wavelet approach to study frequency and amplitude modulation in renal autoregulation. Phys. Rev. E **70**(3), 031915 (2004). https://doi.org/10.1103/PhysRevE.70.031915
36. O.V. Sosnovtseva, A.N. Pavlov, E. Mosekilde, N.-H. Holstein-Rathlou, D.J. Marsh, Double-wavelet approach to studying the modulation properties of nonstationary multimode dynamics. Physiol. Meas. **26**, 351 (2005). https://doi.org/10.1088/0967-3334/26/4/002
37. L.L. Colgin, Theta-gamma coupling in the entorhinal-hippocampal system. Curr. Opin. Neurobiol. **31**, 45–50 (2015). https://doi.org/10.1016/j.conb.2014.08.001
38. P. Sauseng, C. Peylo, A.L. Biel, E.V.C. Friedrich, C. Romberg-Taylor, Does cross-frequency phase coupling of oscillatory brain activity contribute to a better understanding of visual working memory? Br. J. Psychol. **110**, 245–255 (2019). https://doi.org/10.1111/bjop.12340
39. I. Mysin, L. Shubina, From mechanisms to functions: the role of theta and gamma coherence in the intrahippocampal circuits. Hippocampus **32**, 342–358 (2022). https://doi.org/10.1002/hipo.23410
40. Y. Yang, H. Gritton, M. Sarter, S.J. Aton, V. Booth, M. Zochowski, Theta-gamma coupling emerges from spatially heterogeneous cholinergic neuromodulation. PLoS Comput. Biol. **17**, 1009235 (2021). https://doi.org/10.1371/journal.pcbi.1009235
41. H. Noyama, Y. Yoshikai, K. Kotani, Y. Jimbo, Mathematical analysis of multiple spike time series synchronized in phase with collective theta wave using neural cell model. Electron. Commun. Jpn. **104**, 95–102 (2021). https://doi.org/10.1002/ecj.12294
42. Q. Moreau, L. Adel, C. Douglas, G. Ranjbaran, G. Dumas, A neurodynamic model of inter-brain coupling in the gamma band. J. Neurophysiol. (2022). https://doi.org/10.1152/jn.00224.2022

43. S.Y. Makovkin, I.V. Shkerin, S.Y. Gordleeva, M.V. Ivanchenko, Astrocyte-induced intermittent synchronization of neurons in a minimal network. Chaos Solitons Fractals **138**, 109951 (2020). https://doi.org/10.1016/j.chaos.2020.109951
44. A.G. Flesia, P.S. Nieto, M.A. Aon, J.M. Kembro, Computational approaches and tools as applied to the study of rhythms and chaos in biology. In: Computational Systems Biology in Medicine and Biotechnology. Methods and Protocols (Humana, New York, NY, 2022). pp. 277–341. https://doi.org/10.1007/978-1-0716-1831-8_13
45. M. Vaghefi, A.M. Nasrabadi, S.M.R.H. Golpayegani, M.R. Mohammadi, S. Gharibzadeh, Identification of chaos-periodic transitions, band merging, and internal crisis using wavelet-DFA method. Int. J. Bifurc. Chaos **26**, 1650065 (2016). https://doi.org/10.1142/S0218127416500656
46. A.N. Pavlov, O.N. Pavlova, O.V. Semyachkina-Glushkovskaya, J. Kurths, Enhanced multiresolution wavelet analysis of complex dynamics in nonlinear systems. Chaos **31**, 043110 (2021). https://doi.org/10.1063/5.0045859
47. G. Bonciolini, D. Ebi, E. Boujo, N. Noiray, Experiments and modelling of rate-dependent transition delay in a stochastic subcritical bifurcation. Roy. Soc. Open Sci. **5**, 172078 (2018). https://doi.org/10.1098/rsos.172078
48. Y. Yu, Z. Zhang, X. Han, Periodic or chaotic bursting dynamics via delayed pitchfork bifurcation in a slow-varying controlled system. Commun. Nonlinear Sci. Numer. Simul. **56**, 380–391 (2018). https://doi.org/10.1016/j.cnsns.2017.08.019
49. I. Pavithran, R.I. Sujith, Effect of rate of change of parameter on early warning signals for critical transitions. Chaos Interdiscipl. J. Nonlinear Sci. **31**, 013116 (2021). https://doi.org/10.1063/5.0025533
50. T.M. Bury, R.I. Sujith, I. Pavithran, M. Scheffer, T.M. Lenton, M. Anand, C.T. Bauch, Deep learning for early warning signals of tipping points. Proc. Natl. Acad. Sci. USA **118**, 2106140118 (2021). https://doi.org/10.1073/pnas.2106140118